crystals

MDPI

Article

Extended Defect Propagation in Highly Tensile-Strained Ge Waveguides

Meng Qi [1,2], William A. O'Brien [1,3], Chad A. Stephenson [1,4], Victor Patel [1,4], Ning Cao [5], Brian J. Thibeault [5], Marco Schowalter [6], Andreas Rosenauer [6], Vladimir Protasenko [7], Huili (Grace) Xing [7] and Mark A. Wistey [1,*]

1 Electrical Engineering, University of Notre Dame, Notre Dame, IN 46556, USA; mqi1@alumni.nd.edu (M.Q.); wobrien1@alumni.nd.edu (W.A.O.); Chad.A.Stephenson.15@nd.edu (C.A.S.); victorp88@gmail.com (V.P.)
2 Uber, San Francisco, CA 94103, USA
3 Rigetti Quantum Computing, 775 Heinz Avenue, Berkeley, CA 94710, USA
4 Sandia National Laboratory, Albuquerque, NM 87185, USA
5 Electrical and Computer Engineering, University of California, Santa Barbara, CA 93106, USA; ningcao@ece.ucsb.edu (N.C.); thibeault@ece.ucsb.edu (B.J.T.)
6 Institute of Solid State Physics, University Bremen, Otto-Hahn-Allee 1, Bremen 28359, Germany; schowalter@ifp.uni-bremen.de (M.S.); rosenauer@ifp.uni-bremen.de (A.R.)
7 Electrical and Computer Engineering, Cornell University, Ithaca, New York, NY 14853, USA; vvp7@cornell.edu (V.P.); grace.xing@cornell.edu (H.X.)
* Correspondence: markwistey@ieee.org; Tel.: +1-574-631-1639

Academic Editor: Winnie Wong-Ng
Received: 8 March 2017; Accepted: 11 May 2017; Published: 26 May 2017

Abstract: Tensile-strained Ge is a possible laser material for Si integrated circuits, but reports of lasers using tensile Ge show high threshold current densities and short lifetimes. To study the origins of these shortcomings, Ge ridge waveguides with tensile strain in three dimensions were fabricated using compressive silicon nitride (SiN_x) films with up to 2 GPa stress as stress liners. A Raman peak shift of up to 11 cm^{-1} was observed, corresponding to 3.6% hydrostatic tensile strain for waveguides with a triangular cross-section. Real time degradation in tensile-strained Ge was observed and studied under transmission electron microscopy (TEM). A network of defects, resembling dark line defects, was observed to form and propagate with a speed and density strongly correlated with the local strain extracted from both modeled and measured strain profiles. This degradation suggests highly tensile-strained Ge lasers are likely to have significantly shorter lifetime than similar GaAs or InGaAs quantum well lasers.

Keywords: strained germanium; stress liner; tensile strain; direct bandgap; dark line defects; optical waveguide; stability; silicon photonics

1. Introduction

Tensile-strained germanium has been studied as a possible laser material due to its nearly-direct bandgap [1,2] and its compatibility with conventional silicon integrated circuit fabrication [3–6]. Theoretically, a tensile strain of 0.7% (hydrostatic) or 1.4% (biaxial) could produce a direct bandgap in Ge [7–10]. The hydrostatic component of strain is responsible for the shift from an indirect to a direct bandgap. Biaxial strain has a weaker hydrostatic component due to Poisson contraction along the out-of-plane direction.

Many approaches to inducing tensile strain for Ge lasers and more efficient light emitters have been demonstrated [11–19]. The first optically pumped Ge laser used 0.15% biaxial strain plus degenerate n-type doping to partly populate the Γ valley with electrons despite the indirect bandgap [2].

Enhanced electroluminescence from Ge light-emitting diodes (LEDs) has been demonstrated based on tensile-strained Ge with different stressors, but power efficiency needs to be significantly improved for practical lasers [13–16]. Enhanced direct-bandgap photoluminescence has similarly been demonstrated [20–22]. Although electrically-pumped pulsed Ge lasers have been demonstrated, the reported threshold currents were very large and operating lifetimes short [23,24]. Efforts to increase efficiency and optical gain by inducing higher strain are often faced with higher dislocation density and nonradiative recombination, which increases the laser threshold. Also, the high circulating power in lasers can lead to the generation of extended defects in real time. This is observed as dark line defects (DLDs), which are dislocation networks and stacking faults generated in the laser due to high thermal, optical, and electrical power densities [25,26].

To study the stability of highly tensile-strained Ge in the presence of perturbations, this work exposed both strained and unstrained Ge to 300 kV electrons in transmission electron microscopy (TEM). Real-time defect generation observed in transmission electron microscopy (TEM) was then correlated with strain distribution analysis, Raman spectroscopy, and photoluminescence (PL). Tensile strain with a strong hydrostatic component was induced in Ge waveguides by compressive SiN_x stress liners [27,28], which are widely used for strained complementary metal oxide semiconductor (CMOS) transistors. In a wraparound geometry, as shown in Figure 1, compressive stress in the SiN_x induces significant tensile strain up to 3.6% in the Ge along two dimensions, just as planar biaxial strain techniques would do. In addition, the third dimension (longitudinal) is constrained, which enhances the total hydrostatic component of strain by preventing Poisson contraction that occurs in planar techniques.

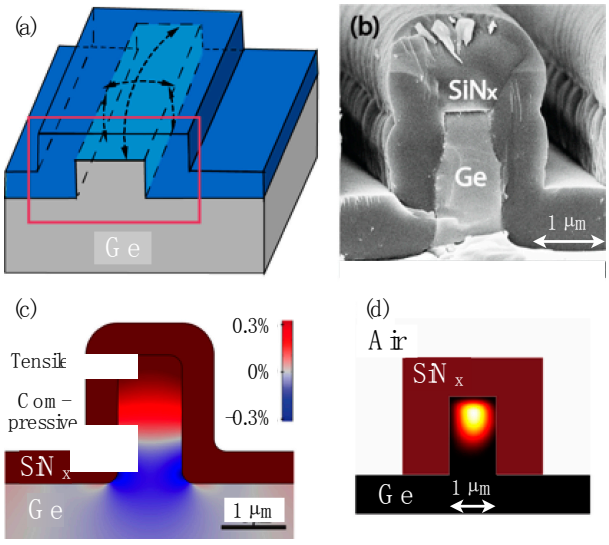

Figure 1. (**a**) Structure of the tensile-strained Ge waveguide. The conformal SiN_x stress liner induces large vertical and lateral strain to the Ge waveguides (arrows) while adding slight tensile strain (longitudinal) due to wafer bowing; (**b**) SEM cross-section of a waveguide covered by a 1 GPa compressive SiN_x film; (**c**) Cross-sectional strain profile simulated by COMSOL for a 1 μm-wide waveguide and a 0.5-μm SiN_x film; (**d**) The calculated optical mode profile with sufficient strain to reach a direct bandgap, approximately 2x that shown in (**c**). Parts (**b**,**c**) © 2012 IEEE. Reprinted, with permission, from *IEEE Proceedings* [1].

2. Results

Figure 2 shows the top-incidence Raman spectrum of the fabricated Ge waveguides. Contributions from the substrate were ruled out by measurements at different locations and focal depths (supplemental Figure S1). The Raman pump laser had a wavelength of 488 nm, with a spot size of ~0.5 μm and a calculated penetration depth around 19 nm in Ge. The system was calibrated using a

reference bulk Si crystal. A shift from the bulk Ge peak of 11 cm^{-1} was observed for waveguides with a strongly (~2 GPa) compressive-strained SiN_x film. This shift in Raman corresponds to a sufficiently high strain, causing an expected direct bandgap and strong photoluminescence (PL) emission, with an effective hydrostatic strain up to 3.6% [29]. We attribute the difference from our COMSOL model to be due to the sharp peak geometry for the narrowest waveguide sample, which focuses strain on a narrow stripe along the top of the waveguide.

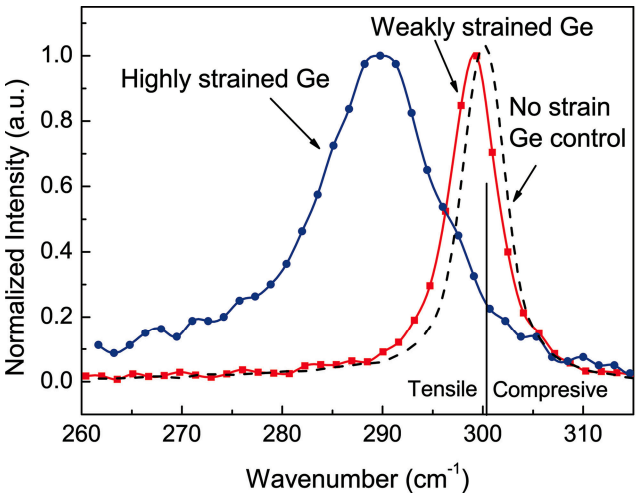

Figure 2. Raman spectra of 0.5 μm wide triangular waveguides under different strains. The highly strained Ge waveguide is stressed by a 1 μm thick, 2 GPa SiN_x compressive-strained film, while the weakly strained Ge is achieved using a 1 μm, 1 GPa SiN_x film plus a 20-nm strain-neutral SiN_x protection layer. The highest observed shift of 11 cm^{-1} was found in the highly strained waveguide, corresponding to 3.6% tensile strain assuming hydrostatic strain. The vertical line shows the location of the peak for bulk Ge, 300.5 cm^{-1}. © 2012 IEEE. Reprinted, with permission, from *IEEE Proceedings* [1].

The high intensity of the laser used in Raman spectroscopy can itself lead to an apparent shift in the peak position. To determine the upper limit on laser power, the power dependence of the Raman spectra was measured both in the far field (Figure 3b) and centered on a strained waveguide (Figure 3c), as shown in Figure 3. Waveguides showed a stronger power dependence than the far field, with a thermal shift of up to -3.5 cm^{-1}, indicating that the tall waveguide geometry was insufficient to dissipate the heat from laser powers >2 mW. Therefore, unless otherwise noted, the Raman measurements in this paper used lower laser powers.

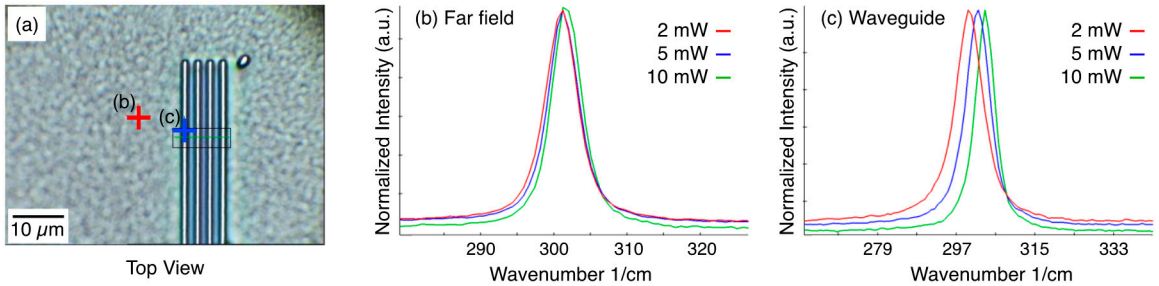

Figure 3. Raman spectroscopy of SiN_x-covered Ge with different laser powers. (**a**) Top view of four adjacent Ge waveguides, showing locations where Raman spectra were acquired for (**b**,**c**). (**b**) Flat surface in far field; (**c**) Centered on strained waveguide.

Figure 4 shows a comparison of normal-incidence PL for different strains. The excitation wavelength was 1310 nm, which has a penetration depth in bulk Ge of 1.5 μm. In the highly strained

waveguides, PL intensity was very weak. Since both Raman and TEM (below) confirm significant strain, the weak PL indicates a large number of non-radiative recombination centers. The sample with a lower (~1 GPa) compressive stress SiN_x film, i.e., weakly strained Ge, had a PL intensity higher than the highly strained Ge but lower than the unstrained control sample; furthermore, a much smaller PL peak wavelength shift was observed.

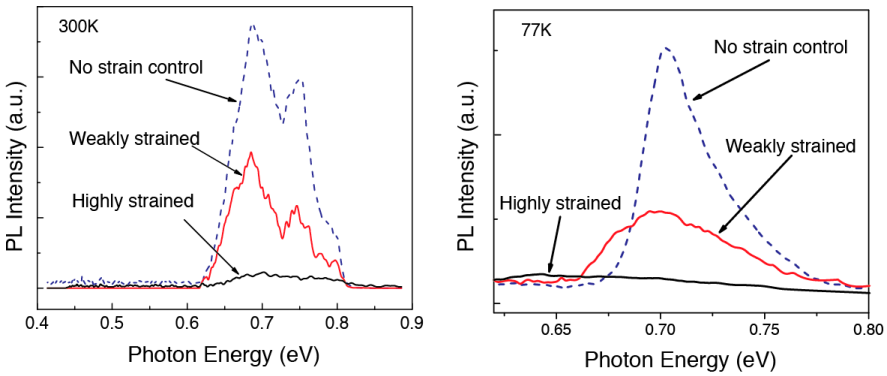

Figure 4. PL from the control sample and the 0.5 μm wide waveguides with different strain values (from no strain to highest tensile strain value), also shown in Figure 2. Little wavelength shift was observed for weakly strained waveguides, while highly strained waveguides had weak PL intensity. 300 K data is © 2012 IEEE and reprinted, with permission, from *IEEE Proceedings* [1].

To understand the reasons for weak PL emission, we used transmission electron microscopy (TEM) to investigate the strained-Ge/SiN_x interface. The highly strained Ge sample is shown in Figure 5. Even using the shortest possible imaging time to acquire focus (~15 s), dark spots were seen near the Ge/SiN_x interface. Smaller but similar spots were observed in all samples with compressive SiN_x, even in the far field where Ge strain was minimal, but more pronounced for higher stress SiN_x, consistent with more intense ion bombardment of the surface during nitride deposition. With increasing electron-beam exposure time, the dark spots grew larger and darker, indicating a more severe structural degradation. To assure the same electron flux for direct comparisons, beam current and magnification were kept as close as possible between samples.

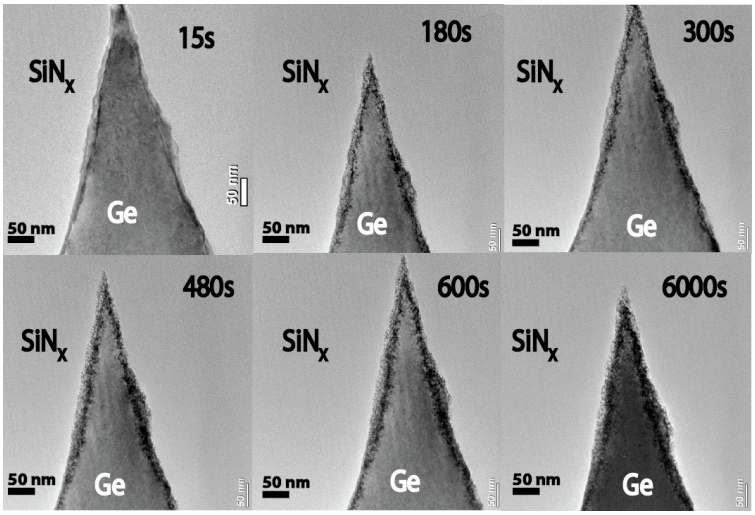

Figure 5. A series of cross-section TEM images at the tip of a triangular waveguide with a 0.5 μm base and 2 GPa strained SiN_x stress liner, for different e-beam exposure times. Darker areas in Ge contain more extended defects. © 2012 IEEE. Reprinted, with permission, from *IEEE Proceedings* [1].

Highly strained Ge was found to degrade rapidly under TEM imaging conditions. To show the time-dependence of the TEM image contrast, a series of TEM images were taken as a function of beam exposure at a constant dose rate, as shown in Figure 6. The damage is compared across different regions by imaging after certain time intervals. There is no degradation for the region where Ge has relaxed or is not intentionally strained, while the degradation is apparently severe near the strained Ge/SiN_x interface. For the highly strained sample, the degraded area quickly increases in size, propagating into the bulk Ge from the Ge/SiN_x interface. In order to obtain a quantitative comparison, the brightness of all images was normalized to that of SiN_x. With dark spots denoting defective areas, the portion of the defective area in the same region (delineated by a dashed box in Figure 6 to account for sample drift) for both low strain and high strain samples is shown as a function of electron exposure time in Figure 7. Defects were observed to propagate faster and deeper for highly strained samples, but progressive degradation was observed for all samples with tensile strain, and no degradation was observed for samples without strain.

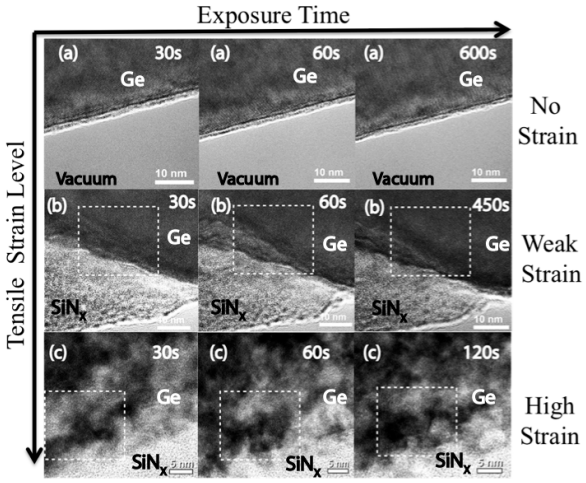

Figure 6. Time-dependent damage study by HRTEM for 0.5 μm wide waveguides with different strains. (**a**) SiN_x/Ge interface has been polished away, with strain assumed completely relaxed. No obvious beam damage was observed; (**b**) SiN_x/Ge interface in a weakly strained waveguide. Weak damage confined within 2–3 nm from the interface was observed, propagating slowly; (**c**) SiN_x/Ge interface in a highly strained waveguide. Severe damage can be found propagating deep into the bulk over a relatively short exposure time. The dashed region was used to track sample drift and calculate the defective area. © 2012 IEEE. Reprinted, with permission, from *IEEE Proceedings* [1].

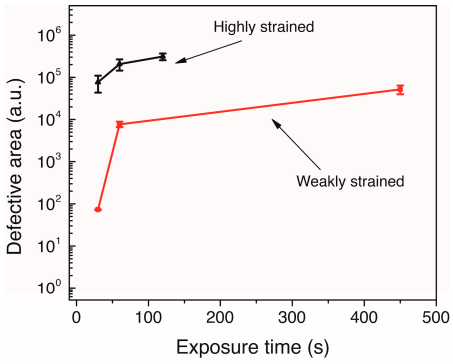

Figure 7. Area of defective region vs. e-beam exposure time for regions delineated in Figure 5b,c. Upon exposure to an electron beam, a defective area rapidly formed at the strained interface and propagated quickly in highly strained waveguides. Defects form relatively slowly in weakly strained waveguides. Unstrained Ge (not shown) showed no visible degradation.

3. Discussion

We attribute the observed degradation to instability in the highly strained Ge. Figure 8 shows a cross-section HRTEM strain analysis for the same sample as Figure 2. Extracted values of tensile strain were comparable with the values from Raman, averaging +3.0% (tensile) along [022] and −1.2% along [0$\bar{2}$2], although quantitative accuracy is limited in this technique due to the large number of defects. Qualitatively, the strain was also found to be non-uniform, with tensile strain highest at the Ge-SiN_x interface. Figure 9 shows that the pattern of degradation follows the distribution of strain calculated using an elastic strain model in COMSOL. No degradation with time (darkening in TEM) was visible in the bulk Ge below the waveguide, where SiN_x would exert little or no strain. Rapid and deep degradation was observed near the tip of the triangular waveguide where the SiN_x stress liner geometry exerts the most strain due to geometry. Intermediate values of strain may only lead to slight darkening near the Ge-SiN_x interface. The figure shows a snapshot of darkening after just 15 s at low magnification, corresponding to a lower dose than previous figures.

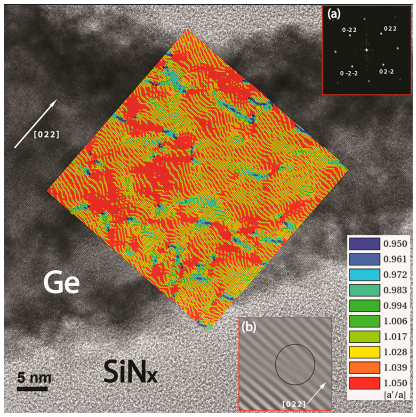

Figure 8. Mapping of strain along [022] on [100] zone axis HRTEM of a triangular Ge corner area in a 0.5 µm wide, highly strained waveguide. The colors indicate the value of the normalized lattice parameter. Upper inset (**a**): Diffraction pattern of the sample. The average tensile strain along [022] direction is 3.0%. Correlation of the non-uniform strain distribution and the darker defective domains can be observed by zooming into a dark spot and using a single diffraction point to image the lattice planes, for example (220), as shown in the lower inset (**b**). The circle highlights an extra half plane at a dislocation.

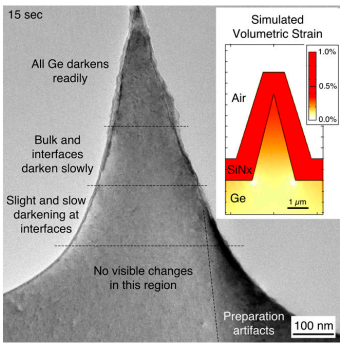

Figure 9. Real-time darkening in TEM [022] occurs in a pattern corresponding with simulated strain. Dashed lines are meant to demarcate regions of different effects, although strain variation is continuous from bottom to top. The dark region at bottom right was due to TEM sample preparation and did not further darken with prolonged beam exposure. Inset: COMSOL elastic strain model of similar triangular waveguide shows zero or slight compressive strain at the bottom of the waveguide and maximum strain near the tip.

Although the theoretical tensile strength of Ge is predicted to be 14–20 GPa [30,31] while undergoing an elastic deformation, experimental measurements range from 15 to 18 GPa [32,33] for Ge nanowires to just 40–95 MPa for bulk Ge [34]. This study indicates that tensile-strained Ge is prone to premature relaxation nucleating at defects, interfaces, or asperities. Achieving sufficient tensile strain to produce a direct bandgap therefore requires extremely gentle fabrication and passivation techniques with no nucleation points for relaxation. Figure 8 indicates that the highly strained Ge degraded in a distinct pattern. The strain analysis in Figure 8 also confirms that the defective areas are networks of dislocations and stacking faults propagating in real time, and that there is a correlation between defective area and strain distribution.

Nucleation of these defects could be driven by energetic fabrication techniques such as ion bombardment during either the reactive ion etching (RIE) or the dual-frequency plasma enhanced chemical vapor deposition (DF-PECVD) of compressive SiN_x. Such damage could then propagate into the strained bulk area during TEM observation. However, the degradation effect was more severe on the top of the waveguide, which received the least exposure to ion bombardment (protected by the mask) during RIE etching but comparable bombardment during SiN_x deposition. Also, dark spots existed at the interface for all samples with strained SiN_x, even in the far field where the Ge was effectively unstrained. Therefore, we attribute this surface damage due to ion bombardment during the nitride deposition. Therefore, we do not believe RIE etching contributed significantly to the sensitivity of the Ge under TEM e-beam exposure.

As mentioned above, the Ge waveguides that had lower strains either due to wider features or lower stress (1 GPa) SiN_x also demonstrated the formation of defects in real time, but at a slower rate. We were unable to establish a threshold of maximum strain for which the defects would not form; they formed in all strained Ge waveguides, but much slower for lower strains. We conclude that the strain necessary to achieve a fully direct bandgap is well beyond the threshold for structural stability in the presence of perturbations such as TEM or, by analogy with DLDs in GaAs/AlGaAs lasers, intense optical illumination [35] and free carrier injection [36,37].

4. Materials and Methods

Ge ridge waveguides with widths from 0.5 μm to 80 μm were patterned by contact lithography on (001) Ge wafers and a 2 μm deep etch by RIE. Due to mask erosion during RIE, the sidewalls of the waveguide were sloped by approximately a 4:1 ratio. The narrowest (0.5 μm) waveguide thus had a triangular cross-section, which enhanced the local strain near the tip of the triangle. Next, 1 μm thick compressive-strained SiN_x stress liners with a stress of either 1 GPa (low strain) or 2 GPa (high strain) were deposited by DF-PECVD. As discussed above, the mechanism for inducing compressive strain in SiNx by DF-PECVD is by ion bombardment, mostly H^+. Figure 1a shows a schematic of the waveguide structure, indicating the components of stress from the SiN_x film applied along the in-plane and out-of-plane directions. Figure 1b shows a scanning electron microscopy (SEM) image of a cleaved fabricated waveguide structure with rectangular cross-section. The strain distribution in the waveguide structure was simulated using *COMSOL Multiphysics*. Figure 1c shows one of the simulated waveguide structures, predicting that the upper region is tensile-strained while the lower regions are under compression. Figure 1d shows the optical mode profile predicted from the strain profile [38]. Cross-section high-resolution TEM (HRTEM) images were taken in a FEI Titan 80–300 TEM system. The strain in fabricated waveguides was characterized by a WITec Alpha 300R confocal Raman microscope system. HRTEM was also used for strain analysis using the Digital Analysis of Lattice Images (DALI) software package [39]. The specimens were tilted along the zone axis for TEM imaging. All the TEM specimens were prepared by focused ion beam (FIB) milling.

5. Conclusions

In summary, highly tensile-strained Ge waveguides were observed to rapidly degrade under the perturbation of an electron beam in TEM, while lower-strained Ge degraded more slowly, and no

degradation was observed in unstrained or compressively strained Ge, even on the same wafer. Although the use of SiN_x stress liners induced tensile strains in the Ge of up to 3.0–3.6%, as measured by Raman and HRTEM strain analysis, and PL peak emission shifted to lower energies, PL emission was very weak. Strain distribution analysis showed a non-uniform strain profile with an average strain of +3.0% (tensile) along [022] and −1.2% (compressive) along [0$\bar{2}$2]. Degradation closely followed the pattern of strain according to TEM strain distribution analysis as well as numerical elastic strain models. Since low-strained Ge and comparably strained InGaAs do not show such rapid degradation, it appears that tensile Ge is more fragile than comparable InGaAs quantum wells for lasers. Specifically, we believe local variations in strain near Ge surfaces or interfaces can lead to the rapid formation of dislocations and stacking faults. The results indicate that tensile Ge is better suited for low-energy devices such as detectors and modulators than it is for lasers, where high optical powers and free carrier recombination will accelerate the formation and propagation of such defects.

Supplementary Materials: The following are available online at www.mdpi.com/2073-4352/7/6/157/s1, Figure S1: Raman spectroscopy at various locations on, near, and far from waveguides.

Acknowledgments: This work was partly supported by the Midwest Institute for Nanoelectronics Discovery (MIND), the National Science Foundation under DMR-1508646, the Notre Dame Office of Research, the Notre Dame Energy Center, and the Notre Dame Integrated Imaging Facility. The authors thank WITec Instruments for 2D Raman strain profiling.

Author Contributions: Meng Qi measured and analyzed TEM and Raman data; William A. O'Brien fabricated waveguides; Ning Cao and Brian J. Thibeault performed DF-PECVD depositions; Chad A. Stephenson simulated strain profiles; Marco Schowalter and Andreas Rosenauer assisted with TEM strain analysis; Victor Patel and Huili (Grace) Xing provided feedback on experimental concepts and manuscript; Mark Wistey originated and supervised the work; Meng Qi and Mark Wistey wrote the manuscript.

Conflicts of Interest: The authors declare no conflict of interest.

References

1. Qi, M.; O'Brien, W.A.; Stephenson, C.A.; Cao, N.; Thibeault, B.J.; Wistey, M.A. Stability of Tensile-Strained Ge Studied by Transmission Electron Microscopy. In Proceedings of the International Silicon-Germanium Technology and Device Meeting (ISTDM), Berkeley, CA, USA, 4–6 June 2012. [CrossRef]
2. Liu, J.; Sun, X.; Camacho-Aguilera, R.; Kimerling, L.C.; Michel, J. Ge-on-Si laser operating at room temperature. *Opt. Lett.* **2010**, *35*, 679–681. [CrossRef] [PubMed]
3. Lieten, R.R.; Bustillo, K.; Smets, T.; Simoen, E.; Ager, J.W.; Haller, E.E.; Locquet, J.-P. Photoluminescence of bulk germanium. *Phys. Rev. B* **2012**, *86*, 035204. [CrossRef]
4. Yang, H.S.; Malik, R.; Narasimha, S.; Li, Y.; Divakaruni, R.; Agnello, P.; Allen, S.; Antreasyan, A.; Arnold, J.C.; Bandy, K.; et al. Dual Stress Liner for High Performance Sub-45 nm Gate Length SOI CMOS Manufacturing. In Proceedings of the IEEE International Electron Devices Meeting, San Francisco, CA, USA, 13–15 December 2004; pp. 1075–1077. [CrossRef]
5. Vincent, B.; Gencarelli, F.; Lin, D.; Nyns, L.; Richard, O.; Bender, H.; Douhard, B.; Moussa, A.; Merckling, C.; Witters, L.; et al. Biaxial and Uniaxial Compressive Stress Implemented in Ge(Sn) pMOSFET Channels by Advanced Reduced Pressure Chemical Vapor Deposition Developments. *ECS Trans.* **2011**, *41*, 239–248. [CrossRef]
6. Eneman, G.; Hellings, G.; Mitard, J.; Witters, L.; Yamaguchi, S.; Bardon, M.G.; Christie, P.; Ortolland, C.; Hikavyy, A.; Favia, P.; et al. $Si_{1-x}Ge_x$-Channel PFETs: Scalability, Layout Considerations and Compatibility with Other Stress Techniques. *ECS Trans.* **2011**, *35*, 493–503. [CrossRef]
7. Fischetti, M.V.; Laux, S.E. Band structure, deformation potentials, and carrier mobility in strained Si, Ge, and SiGe alloys. *J. Appl. Phys.* **1996**, *80*, 2234–2252. [CrossRef]
8. Aldaghri, O.; Ikonic´, Z.; Kelsall, R.W. Optimum strain configurations for carrier injection in near infrared Ge lasers. *J. Appl. Phys.* **2012**, *111*, 053106. [CrossRef]
9. Boztug, C.; Sanchez-Perez, J.R.; Sudradjat, F.F.; Jacobson, R.; Paskiewicz, D.M.; Lagally, M.G.; Paiella, R. Tensilely strained germanium nanomembranes as infrared optical gain media. *Small* **2013**, *9*, 622. [CrossRef] [PubMed]

10. Scopece, D.; Montalenti, F.; Bollani, M.; Chrastina, D.; Bonera, E. Straining Ge bulk and nanomembranes for optoelectronic applications: A systematic numerical analysis. *Semicond. Sci. Technol.* **2014**, *29*, 095012. [CrossRef]
11. Huo, Y.; Lin, H.; Chen, R.; Makarova, M.; Rong, Y.; Li, M.; Kamins, T.I.; Vuckovic, J.; Harris, J.S. Strong enhancement of direct transition photoluminescence with highly tensile-strained Ge grown by molecular beam epitaxy. *Appl. Phys. Lett.* **2011**, *98*, 011111. [CrossRef]
12. Bai, Y.; Lee, K.E.; Cheng, C.; Lee, M.L.; Fitzgerald, E.A. Growth of highly tensile-strained Ge on relaxed $In_xGa_{1-x}As$ by metal-organic chemical vapor deposition. *J. Appl. Phys.* **2008**, *104*, 084518. [CrossRef]
13. Sun, X.; Liu, J.; Kimerling, L.C.; Michel, J. Room-temperature direct bandgap electroluminesence from Ge-on-Si light-emitting diodes. *Opt. Lett.* **2009**, *34*, 1198–1200. [CrossRef] [PubMed]
14. Kasper, E.; Oehme, M.; Aguirov, T.; Werner, J.; Kittler, M.; Schulze, J. Room Temperature Direct Band Gap Emission from Ge p-i-n Heterojunction Photodiodes. *Adv. Optoelectron.* **2012**, *2012*, 916275. [CrossRef]
15. Nam, D.; Sukhdeo, D.; Cheng, S.; Roy, A.; Huang, K.C.; Brongersma, M.; Nishi, Y.; Saraswat, K. Electroluminescence from strained germanium membranes and implications for an efficient Si-compatible laser. *Appl. Phys. Lett.* **2012**, *100*, 131112. [CrossRef]
16. Oehme, M.; Gollhofer, M.; Widmann, D.; Schmid, M.; Kaschel, M.; Kasper, E.; Schulze, J. Direct bandgap narrowing in Ge LED's on Si substrates. *Opt. Express* **2013**, *21*, 2206–2211. [CrossRef] [PubMed]
17. Süess, M.J.; Geiger, R.; Minamisawa, R.A.; Schiefler, G.; Frigerio, J.; Chrastina, D.; Isella, G.; Spolenak, R.; Faist, J.; Sigg, H. Analysis of enhanced light emission from highly strained germanium microbridges. *Nat. Photonics* **2013**, *7*, 466–472. [CrossRef]
18. Oda, K.; Okumura, T.; Kasai, J.; Kako, S.; Iwamoto, S.; Arakawa, Y. Crystallinity improvements of Ge waveguides fabricated by epitaxial lateral overgrowth. *Jpn. J. Appl. Phys.* **2016**, *55*, 04EH06. [CrossRef]
19. Kasper, E.; Oehme, M.; Werner, J.; Aguirov, T.; Kittler, M. Direct band gap luminescence from Ge on Si pin diodes. *Front. Optoelectron.* **2012**, *5*, 256–260. [CrossRef]
20. Kawamura, Y.; Huang, K.C.Y.; Thombare, S.V.; Hu, S.; Gunji, M.; Ishikawa, T.; Brongersma, M.L.; Itoh, K.M.; McIntyre, P.C. Direct-gap photoluminescence from germanium nanowires. *Phys. Rev. B* **2012**, *86*, 035306. [CrossRef]
21. El Kurdi, M.; De Kersauson, M.; David, S.; Checoury, X.; Beaudoin, G.; Jakomin, R.; Sagnes, I.; Sauvage, S.; Fishman, G.; Boucaud, P. Stimulated emission in single tensile-strained Ge photonic wire. In Proceedings of the 8th IEEE Group IV Photonics (GFP) International Conference, London, UK, 14–16 September 2011. [CrossRef]
22. Jung, D.; Faucher, J.; Mukherjee, S.; Akey, A.; Ironside, D.J.; Cabral, M.; Sang, X.; Lebeau, J.; Bank, S.R.; Buonassisi, T.; et al. Highly tensile-strained Ge/InAlAs nanocomposites. *Nat. Commun.* **2017**, *8*, 14204. [CrossRef] [PubMed]
23. Camacho-Aguilera, R.E.; Cai, Y.; Patel, N.; Bessette, J.T.; Romagnoli, M.; Kimerling, L.C.; Michel, J. An electrically pumped germanium laser. *Opt. Express* **2012**, *20*, 11316. [CrossRef] [PubMed]
24. Koerner, R.; Oehme, M.; Gollhofer, M.; Schmid, M.; Kostecki, K.; Bechler, S.; Widmann, D.; Kasper, E.; Schulze, J. Electrically pumped lasing from Ge Fabry-Perot resonators on Si. *Opt. Express* **2015**, *23*, 14815–14822. [CrossRef] [PubMed]
25. Frank, W.; Gösele, U. A unifying interpretation of dark line defects in GaAs and bright dislocation halos in GaP. *Physica B+C* **1983**, *116*, 420–424. [CrossRef]
26. Bonard, J.-M.; Ganière, J.-D.; Vanzetti, L.; Paggel, J.J.; Sorba, L.; Franciosi, A.; Hervé, D.; Molva, E. Combined transmission electron microscopy and cathodoluminescence studies of degradation in electron-beam-pumped $Zn_{1-x}Cd_xSe/ZnSe$ blue-green lasers. *J. Appl. Phys.* **1998**, *84*, 1263–1273. [CrossRef]
27. Capellini, G.; Reich, C.; Guha, S.; Yamamoto, Y.; Lisker, M.; Virgilio, M.; Ghrib, A.; El Kurdi, M.; Boucaud, P.; Tillack, B.; et al. Tensile Ge microstructures for lasing fabricated by means of a silicon complementary metal-oxide-semiconductor process. *Opt. Express* **2014**, *22*, 399–410. [CrossRef] [PubMed]
28. Kuroyanagi, R.; Nguyen, L.M.; Tsuchizawa, T.; Ishikawa, Y.; Yamada, K.; Wada, K. Local bandgap control of germanium by silicon nitride stressor. *Opt. Express* **2013**, *21*, 18553–18557. [CrossRef] [PubMed]
29. Takai, M.; Tanigawa, T.; Miyauchi, M.; Nakashima, S.; Gamo, K.; Namba, S. Residual Strain in Single Crystalline Germanium Islands on Insulator. *Jpn. J. Appl. Phys.* **1984**, *23*, L363–L365. [CrossRef]
30. Roundy, D.; Cohen, M.L. Ideal strength of diamond, Si, and Ge. *Phys. Rev. B* **2001**, *64*, 212103. [CrossRef]
31. Macmillan, N.H. The theoretical strength of solids. *J. Mater. Sci.* **1972**, *7*, 239–254. [CrossRef]

32. Ngo, L.T.; Almécija, D.; Sader, J.E.; Daly, B.; Petkov, N.; Holmes, J.D.; Erts, D.; Boland, J.J. Ultimate-Strength Germanium Nanowires. *Nano Lett.* **2006**, *6*, 2964–2968. [CrossRef] [PubMed]
33. Smith, D.A.; Holmberg, V.C.; Korgel, B.A. Flexible germanium nanowires: ideal strength, room temperature plasticity, and bendable semiconductor fabric. *ACS Nano* **2010**, *4*, 2356–2362. [CrossRef] [PubMed]
34. Claeys, C. *Germanium-Based Technologies: From Materials to Devices*; Elsevier Science: Oxford, UK, 2007.
35. Monemar, B.; Woolhouse, G.R. Observation and analysis of very rapid optical degradation of GaAs/GaAlAs DH laser material. *Appl. Phys. Lett.* **1976**, *29*, 605–607. [CrossRef]
36. Hasegawa, Y.; Egawa, T.; Jimbo, T.; Umeno, M. Influences of Dark Line Defects on Characteristics of AlGaAs/GaAs Quantum Well Lasers Grown on Si Substrates. *Jpn. J. Appl. Phys.* **1995**, *34*, 2994–2999. [CrossRef]
37. Kamejima, T.; Ishida, K.; Matsui, J. Injection-Enhanced Dislocation Glide under Uniaxial Stress in GaAs–(GaAl)As Double Heterostructure Laser. *Jpn. J. Appl. Phys.* **1977**, *16*, 233–240. [CrossRef]
38. Stephenson, C.S.; O'Brien, W.A.; Wistey, M.A. Tensile Ge Waveguide Designs for Compact Silicon Photonics. In preparation.
39. Rosenauer, A.; Remmele, T.; Gerthsen, D.; Tillmann, K.; Förster, A. Atomic scale strain measurements by the digital analysis of high-resolution transmission electron microscopic lattice images. *Optik* **1997**, *105*, 99.